Wind Estimation based on Flight Dynamics of Unmanned Aerial Vehicle: Influencing Variables and Its Environmental Application

Dukun Chen[1,2], Weifeng Su[1], Shaojie Jiang[1,3], Honglong Yang[5], Chunsheng Zhang[5], Shutong Jiang[6], Dongyang Chang[6], Yuxin Liang[1], Hao Wang[7], Xin Yang[1], Tzung-May Fu[1], Zhenzhong Zeng[1], Lei Zhu[1], Huizhong Shen[1], Chen Wang[1], Jianhuai Ye[1,2,4,*]

[1]State Key Laboratory of Soil Pollution Prevention and Remediation for Soil Security, Southern University of Science and Technology, Shenzhen 518055, China

[2]Shenzhen Key Laboratory of Precision Measurement and Early Warning Technology for Urban Environmental Health Risks, School of Environmental Science and Engineering, Southern University of Science and Technology, Shenzhen 518055, China

[3]Jiangsu Key Laboratory of Atmospheric Environment Monitoring and Pollution Control, School of Environmental Science and Engineering, Nanjing University of Information Science and Technology, Nanjing, 210000, China

[4]Guangdong Provincial Observation and Research Station for Coastal Atmosphere and Climate of the Greater Bay Area, Shenzhen, 518055, China

[5]Shenzhen National Climate Observatory, Meteorological Bureau of Shenzhen Municipality, Shenzhen 518040, China

[6]Soarability Pte. Ltd., Singapore 409051, Singapore

[7]Shenzhen Key Laboratory for Air Vehicle and Gust Simulation, School of Mechanics and Aerospace Engineering, Southern University of Science and Technology, Shenzhen 518055, China

[*]*Correspondence to*: Jianhuai Ye (yejh@sustech.edu.cn)

Submitted to *Atmospheric Chemistry and Physics*

Abstract. Accurate wind measurement is critical for atmospheric and environmental sciences; however, achieving high spatiotemporal resolution with operational flexibility remains challenging. This study develops and validates an approach for estimating horizontal wind speed and direction based on the flight dynamics of an unmanned aerial vehicle (UAV). Through controlled wind wall experiments, we established a relationship between UAV attitude (e.g., roll, pitch, and yaw) and wind speed. This relationship varies significantly with relative wind direction (with respect to UAV orientation) and payload configuration due to the built-in flight control system and asymmetric airframe of the UAV deployed, demonstrating the necessity of platform-specific calibration for practical application. The performance of this attitude-based method was compared against measurements from a calibrated onboard ultrasonic anemometer. While the sensor-based method achieved good accuracy for hovering and low-speed vertical flights, its performance degraded at higher vertical speeds (>2 m/s) due to rotor-induced airflow interference. In contrast, the attitude-based method maintained robust accuracy across all flight regimes. Furthermore, a machine learning model was developed to deliver high-fidelity wind estimates (R^2 > 0.90). The model integrated attitude data, flight dynamics, and environmental parameters (e.g., air pressure) and was trained on data from UAV flights during a 20-day field campaign. Validation against measurements from a meteorological tower confirmed the reliability of the machine learning method. This work presents a sensor-free, computationally efficient framework for obtaining high-resolution wind data. By addressing the critical, platform-specific factors affecting estimation accuracy, our approach enhances the applicability of UAVs for advanced environmental monitoring, atmospheric research, and safety assessments in the emerging low-altitude economy.

TOC

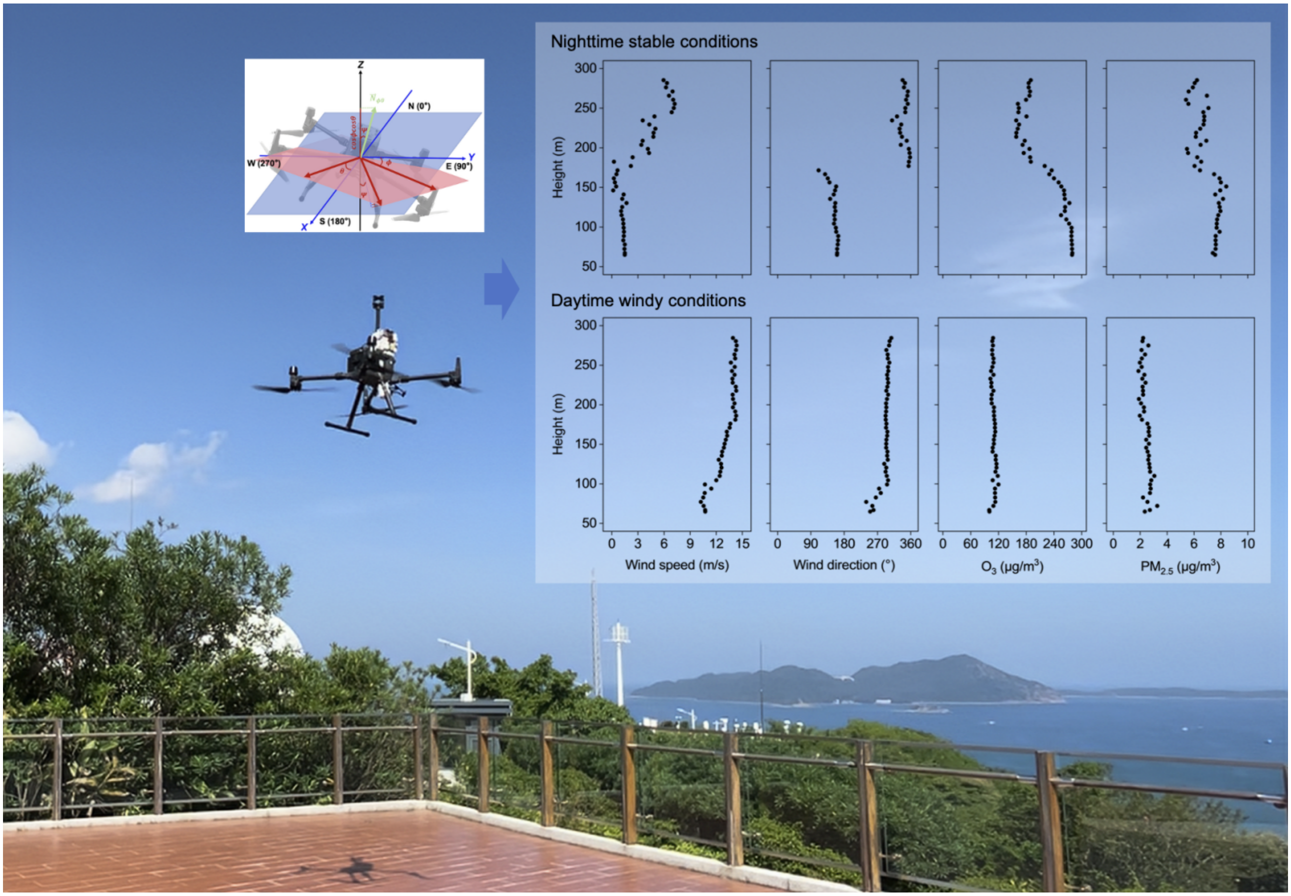

Nighttime stable conditions
Daytime windy conditions
Height (m)
Wind speed (m/s)
Wind direction (°)
O3 (µg/m3)
PM2.5 (µg/m3)
N (0°)
E (90°)
S (180°)
W (270°)

1. Introduction

Wind speed and direction are among the most fundamental and critical observational elements in atmospheric and environmental sciences (Horton et al., 2014; Wang and Chen, 2016; Guo et al., 2016; Yang et al., 2016; Yang et al., 2017). Accurate measurement of these parameters is vital across fields such as weather forecasting, pollution monitoring, and urban planning (Salmabadi et al., 2020; Tominaga and Shirzadi, 2021; Alizadeh et al., 2022; Curbelo and Rypina, 2023; Yang et al., 2025a). For instance, wind directly influences the development and evolution of weather systems and serves as an essential parameter for numerical weather predictions (Salmabadi et al., 2020; Alizadeh et al., 2022). Real-time wind data coupled with atmospheric dispersion models can predict the spread of toxic gases from industrial emissions (Yang et al., 2025a) or smoke plume trajectories from fires (Curbelo and Rypina, 2023), which enables authorities to issue timely health advisories and coordinate emergency responses. For urban planning, wind patterns significantly influence thermal distribution within urban environments (Tominaga and Shirzadi, 2021). Strategic urban design incorporating prevailing wind speed and direction can optimize ventilation corridors and building layouts to enhance airflow, mitigate heat accumulation, and improve pollutant dispersion.

Achieving high spatiotemporal-resolution wind measurements poses a significant challenge. Traditionally, wind observations have been obtained using techniques that include mechanical instruments (cup and vane types), optical methods (laser Doppler), ultrasonic sensors, and remote-sensing platforms (e.g., satellite and radar). These methods vary considerably in their accuracy, cost, and environmental suitability. For example, cup and vane anemometers are widely used in meteorological and wind energy applications due to their structural simplicity and cost-effectiveness; however, their performance is limited by turbulence sensitivity, dynamic response lag due to inherent mechanical inertia, and reduced accuracy in low air-density environments (Pindado et al., 2014; Alfonso-Corcuera et al., 2022). Optical-based systems, while offering microscale resolution and multi-directional capability, require stringent deployment conditions owning to their high costs and sensitivity to light propagation conditions (Lee, 2003; Diasinos et al., 2013; Knöller et al., 2024). Ultrasonic sensors can achieve high precision through non-mechanical design and wide measurement range, but they are vulnerable to temperature and humidity variations and have multipath interference (Han et al., 2008; Richiardone et al., 2012; Gaeta Lopes et al., 2017; Shan et al., 2023). Finally, remote sensing technologies such as satellite observations provide global coverage for large-scale circulation studies but suffer from fine spatiotemporal resolution limitations (Feng et al., 2023; Hauser et al., 2023).

In recent years, unmanned aerial vehicles (UAVs) have shown broad application potential in atmospheric and environmental sciences, owing to their advantages of low cost, flexible deployment, and the ability to acquire high-resolution three-dimensional data (Batista et al., 2019; Zhao et al., 2021; Ye et al., 2021; Asher et al., 2021; Ye et al., 2022; Achermann et al., 2024; Li et al., 2025). Among UAV platforms, multi-copters are increasingly prominent for wind measurement (Neumann and Bartholmai, 2015; González-Rocha et al., 2023; Ahmed et al., 2024). Their ability to hover and perform vertical profiling at fixed locations provides a key advantage over fixed-wing UAVs for high-resolution atmospheric measurements (Li et al., 2025).

Current wind estimation using copter-type UAVs is primarily based on three technical paradigms. The first approach involves direct measurement with onboard sensors like anemometers. However, this method is often subject to challenges such as signal interference from rotor-induced turbulence and reduced measurement accuracy during UAV tilt maneuvers (Liu et al., 2023; Yang et al., 2025b). The second approach utilizes mechanical model-based estimation, reconstructing wind fields by analyzing UAV flight status. Representative models include the dynamic particle model, kinematic particle model, and rigid body model (Sikkel et al., 2016; González-Rocha et al., 2019, 2023; Ahmed et al., 2024). While these methods can provide accurate wind estimates, they are computationally expensive and struggle to precisely model UAV-wind interactions under complex atmospheric conditions.

The third paradigm employs a data-driven approach, establishing empirical relationships between wind characteristics and UAV flight attitude (e.g., roll, pitch, and yaw). This method offers significant advantages, as it eliminates the need for additional sensors and simplifies system integration, thereby reducing cost, payload weight, and power consumption while enhancing flight endurance and maneuverability. Previous studies have developed algorithms based on this approach and applied them to atmospheric wind estimation (Neumann and Bartholmai, 2015; Brosy et al., 2017; Palomaki et al., 2017). However, critical factors influencing the estimation accuracy of this method, such as payload characteristics (size and placement), rotor-induced effects, and the relative UAV-wind orientation (especially for asymmetric airframes), remain understudied. These parameters significantly influence UAV attitude dynamics and, consequently, the reliability of wind estimates. In addition, existing studies predominantly focus on wind estimation during hovering or horizontal flights, paying insufficient attention to vertical wind variability. This gap is particularly significant for research on air pollutant dispersion and boundary layer dynamics.

This study combines laboratory wind wall experiments with field campaigns (Figures 1A-1C), aiming to systematically examine how the aforementioned factors affect attitude-based wind estimation and to evaluate the feasibility of using this approach for real-world vertical wind profiling. Unless otherwise noted, "wind estimation" in this study refers to the estimation of the horizontal wind components. Results of this study are expected to improve the accuracy, robustness, and operational relevance of UAV-based wind sensing for atmospheric research and environmental monitoring.

2. Methods

2.1 UAV platform

A quadcopter UAV (DJI M300 RTK) was used in this study. It has dimensions of 810 × 670 × 430 mm^3 (L × W × H) when unfolded. The weight of the UAV is 6.3 kg with batteries. The maximum flight weight of the payload is 2.7 kg, and the maximum flight time is 55 min. The maximum ascent and descent speeds of the UAV reach 6 m/s and 5 m/s, respectively. The hovering accuracy ranges from 0.1 to 0.5 m, and the maximum tolerable wind speed is 12 m/s. The UAV is equipped with an inertial measurement unit and a GPS positioning system, which can output the attitude and flight dynamics information required for wind estimation.

2.2 Wind measurement and estimation

UAV-based wind measurements and estimations were conducted at the Laboratory for Air Vehicle and Gust Simulation facility at Southern University of Science and Technology (Shenzhen, China) (Figure 1A). The laboratory features a specialized wind wall system capable of producing stable, controllable airflow conditions. The system can simulate wind shear and gust spectra corresponding to wind speeds up to 15 m/s in controlled environments. During the wind wall experiments, twelve wind speed levels were used by increasing the system power in 5% increments from 1 m/s to 10 m/s (corresponding to specific wind speeds of 1.4 m/s, 2.2 m/s, 3.0 m/s, 3.8 m/s, 4.5 m/s, 5.3 m/s, 6.1 m/s, 6.9 m/s, 7.7 m/s, 8.5 m/s, 9.2 m/s, and 10.0 m/s). Prior to testing, the wind wall output was calibrated using a high-accuracy reference anemometer to ensure measurement reliability.

Three different UAV payload configurations were tested to simulate real-world operational conditions, including a default setup with only a wind sensor (M_o), a configuration with an additional payload of approximately 1.5 kg (160 × 100 × 90 mm^3, L × W × H) mounted at the front-top of the UAV (M_{o+f}), and a configuration with the same payload mounted at the center-top (M_{o+m}), as illustrated in Figure 1D. In order to assess the effects of wind direction relative to the UAV heading on attitude response and wind estimation, six wind directions were explored, including 0°, 45°, 90°, 180°, 225°, and 270°, as illustrated in Figure 1E. For each combination of wind speed and direction, the UAV maintained a stable hover for over 1 min. This procedure yielded a set of relationships between UAV attitude and wind components.

a. Wind estimation based on UAV attitude dynamics (method 1)

UAV tilts in the presence of wind during flights. The inclination angle (Ψ) of the UAV during flight (Figure 2) can be calculated using equation (1):

$$\Psi = arccos(cos\phi cos\theta) \quad (1)$$

where ϕ and θ are the roll (Figure 2A) and pitch (Figure 2B) angles of the UAV, respectively; $cos\phi cos\theta$ corresponds to the projection of the body-axis vertical component of the UAV onto the ground vertical axis (Z-axis) (Figure 2D).

Increasing wind speed causes greater tilt of the UAV. The inclination angle, derived from the roll and pitch angles, is therefore expected to increase with wind speed. The specific functional relationship between the inclination angle and the true wind speed can be then determined empirically by correlating the measured inclination angle with the independently controlled wind speed from the wind wall system (Neumann and Bartholmai, 2015; Brosy et al., 2017).

For wind direction (η_{wind}), it can be estimated based on the UAV attitude using equation (2):

$$\eta_{wind} = \begin{cases} arctan(\frac{-sin\phi cos\theta}{cos\phi sin\theta}) + \delta + 180°, & if\ cos\phi sin\theta > 0; \\ arctan(\frac{-sin\phi cos\theta}{cos\phi sin\theta}) + \delta, & if\ cos\phi sin\theta < 0; \end{cases} \quad (2)$$

where $sin\phi cos\theta$ and $cos\phi sin\theta$ represent the wind components along the Y-axis and X-axis (Figure 2E), respectively. η_r, representing wind direction relative to UAV yaw orientation, can be obtained using equation (3):

$$\eta_r = \delta - \eta_{wind} \quad (3)$$

In this study, η_r was set to 0°, 45°, 90°, 180°, 225°, and 270° during the wind wall experiments, as illustrated previously.

b. Wind estimation based on onboard wind sensor (method 2)

Wind speed and direction data were also obtained directly from a compact and lightweight ultrasonic anemometer (LI-550 TriSonica Mini, LI-COR) mounted on the UAV airframe. The anemometer determines wind parameters by measuring ultrasonic pulse transit time differences along three orthogonal axes. The accuracy of the anemometer is ± 0.2 m/s for speeds between 0 and 10 m/s, and ± 2 % for speeds from 10 m/s to 30 m/s. The wind direction measurement range is 0 to 360°, with a manufacturer-specified sensor accuracy of ± 1°. Data were recorded at 1 Hz by an onboard datalogger during the experiments.

Prior to field deployment, the sensor underwent extensive laboratory calibration in the wind wall facility. Calibration procedures systematically tested wind speeds from 1 to 10 m/s under three payload configurations (baseline, front-loaded, and center-loaded), while also evaluating directional response at six headings relative to the UAV (Figures 1D and 1E). This process generated detailed correction curves that accounted for rotor interference and airframe effects.

c. Wind estimation using a machine learning algorithm (method 3)

A random forest model was also developed for efficient wind estimation. The simulations utilized *RandomForestRegressor* from a Python package (*sci-kit learn*). The number of decision trees was set to 100 to ensure ensemble diversity. Maximum tree depth was not restricted to capture complex data patterns. An 80:20 training-test data split and 10-fold cross-validation were applied. The random seed was fixed at 42 to guarantee the reproducibility of the results.

Model training and validation employed a dataset collected during a summer field campaign at Xichong in Shenzhen, China (Figure 1C). This is a coastal site usually selected for atmosphere-land-ocean interactions. The dataset contained measurements from 20 days (from August 21 to September 14, 2022) with 6 hovering flights conducted each day, specifically 2 flights each during morning, afternoon, and evening periods. Model inputs included UAV attitude parameters (roll, pitch, and yaw) along with supplementary flight data such as UAV flight speed, rotor thrusts, and air pressure. UAV flight speed was derived from onboard GPS measurements, and rotor thrusts were approximated from flight command values (Text S1, Supporting Information). The training targets were obtained from calibrated onboard ultrasonic anemometer measurements (method 2), with performance benchmarks established through comparison against attitude-based wind estimation (method 1).

Performance of the random forest estimation was evaluated using the correlation coefficient (R^2) and root mean squared error (RMSE).

2.3 UAV wind estimation validation

Validation of UAV wind estimation was conducted at the Shiyan Meteorological Gradient Observation Tower in Shenzhen, China (Figure 1B). The tower features 13 external platforms for conventional meteorological measurements. Meteorological measurement platforms are distributed at 10 m, 20 m, 40 m, 50 m, 80 m, 100 m, 150 m, 160 m, 200 m, 250 m, 300 m, 320 m, and 350 m above local ground, providing multi-level wind speed and direction data. Due to flight restrictions in the area where the maximum permissible height was 120 m, flight experiments were conducted within 100 m. Both hovering and vertical flight profiles were performed. For the hovering experiment, UAV with the default payload configuration (M_o) maintained a stationary position for approximately 10 min at an altitude of 100 m above ground level. The vertical flight experiments assessed two payload configurations (M_o and M_{o+f}) at flight speeds of 0.5 m/s and 2.0 m/s. For each configuration and speed, two complete round-trip cycles were performed, ascending from ground level to 100 m and descending back to 0 m. All UAV flights were conducted at a minimum horizontal distance of 20 m from the tower to avoid the disturbance of UAV-induced air flows to the tower measurements.

3. Results and Discussion

3.1 UAV-based wind estimation

a. Estimation based on UAV attitude dynamics (method 1)

Accurate and fast wind estimation requires UAV attitude to respond rapidly to wind change. As shown in Figure S1, which plots UAV inclination angle and controlled wind speed against time for a test flight, wind speed was increased in a stepwise fashion at 15-s intervals. The data, sampled at 1-s intervals, show that the UAV attitude (quantified by the inclination angle) adjusts to each new wind speed level within the first second of the change. This rapid response is evident across all step increments and becomes particularly pronounced at higher wind speeds, indicating a transient response time on the order of 1 s or less for this platform when reacting to a sudden change in wind forcing.

The relationship between UAV inclination angle and wind speed was then modelled using datasets collected under different payload (M) and relative wind direction (η_r) conditions, as presented in Figure 3. Several fitting algorithms were evaluated, including power, logarithmic power, polynomial, and exponential functions. Among these, the power function demonstrated the best fit to the experimental data, which is expressed as:

$$V_{wind,M,\eta_r} = a_{M,\eta_r} \Psi^{b_{M,\eta_r}} \quad (4)$$

where a_{M,η_r} and b_{M,η_r} are fitting coefficients obtained from the wind wall experiments. Overall, the fittings effectively captured the relationship between UAV inclination angle and wind speed (R^2 > 0.85, Table S1).

As shown in Figure 3, the attitude-wind relationship varies significantly with relative wind direction. At identical wind speeds, inclination angles were consistently smaller for headwind to crosswind conditions (0°-90°) than for tailwind to rear crosswind scenarios (180°-270°). This behavior can be attributed to the advanced flight control system of the UAV used in this study. Under headwind conditions, the flight controller proactively compensates for wind disturbances by precisely adjusting front rotor power, inducing a slight forward tilt. This active posture control leverages aerodynamic drag components to enhance stability, thereby minimizing attitude fluctuations (Ding and Wang, 2018; Otsuka et al., 2018; Lei and Lin, 2019; Jung, 2024). Conversely, during tailwind conditions, turbulent flow enveloping the airframe introduces control latency, forcing the system to apply larger attitude corrections to maintain position, ultimately amplifying the observed inclination (Ding and Wang, 2018; Otsuka et al., 2018; Lei and Lin, 2019; Jung, 2024). Adding extra payload generally reduced sensitivity of UAV inclination to wind, leading to smaller observed inclination angles (Figures 3B and 3C versus Figure 3A). And this effect varied slightly with payload placement.

The above findings differ from observations by Neumann and Bartholmai (2015), who reported that payload and wind direction had minimal effects on UAV attitude. This discrepancy likely stems from differences in UAV platforms, including variations in design and flight control architectures. The implication is that UAV attitude-based wind estimation requires specific algorithms tailored to the characteristics of each UAV platform.

b. Estimation based on onboard wind sensor (method 2)

The wind sensor was calibrated during wind wall experiments. Across varying payload configurations and wind directions, linear relationships were observed between sensor-measured wind speeds and the reference wind speeds generated by the wind wall (Figure 4). The coefficients of these linear fits are provided in Table S2.

As shown in Figure 4, sensor measurements exhibited deviations of 30%, 15%, and 30% for the default, front payload, and central payload configurations, respectively. The front payload configuration notably improved measurement accuracy by reducing flight vibrations and enhancing stability (Figure 4B versus Figures 4A and 4C), consistent with the UAV flight control system behavior described in Section 3.1a. In addition, the asymmetric sensor placement on the right front of the UAV (viewed when facing the UAV, Figure 1E) led to maximum accuracy degradation at 225° (rear direction relative to the UAV centerline).

Over the course of the experiments, the sensor registered non-zero wind speed readings even when the actual external wind speed was 0 m/s. The intercepts of the calibration curves for different flight configurations represent the zero bias (Figure 4). This phenomenon can be attributed to the rotor-induced airflow interference. During testing under various payload configurations and wind directions, UAV rotors generated apparent wind speeds ranging from 0.1 to 1.5 m/s (Figure 4). Similarly, the rotor interference effects on sensor measurements were most pronounced when wind approached from the right rear direction (225°) relative to the UAV centerline, likely due to uneven payload distribution.

The implication of these findings is that the sensor cannot be used for field measurements without calibration, and calibration may vary significantly with UAV model used, sensor placement, payload distribution and mass, and relative wind direction during operation.

3.2 Validation of UAV-based wind estimation against tower measurements

The UAV-based wind estimation was validated against observations from the meteorological tower. Results of hovering flight experiments are presented in Figure 5. Wind speeds obtained from method 1 (UAV-attitude based) and method 2 (sensor-based) were generally consistent with each other (Figure 5A). Both methods also closely matched the reference wind speed and direction recorded by the tower-mounted anemometers (Figures 5B and 5C). The difference between the estimation from method 1 and the anemometer readings was less than 0.7 m/s for wind speed and 20° for wind direction, confirming the accuracy and reliability of the UAV-based wind estimation under real-world atmospheric conditions.

The situation changes during vertical flight operations. In this study, vertical flights were conducted at two speeds (i.e., 0.5 m/s and 2 m/s). As shown in Figure 6, wind speeds calculated using method 1 still exhibited strong agreement with meteorological tower measurements, regardless of whether the UAV ascended or descended at 0.5 m/s (Figure 6A-I) or 2.0 m/s (Figure 6B-I). For the sensor-based method (method 2), the measurements matched the tower data at the lower vertical speed (0.5 m/s, Figure 6A-II). However, when the vertical speed increased to 2.0 m/s, significant deviations became apparent (Figure 6B-II). These discrepancies are likely caused by increased rotor-induced turbulence during high-speed vertical flight, which degrades sensor measurement accuracy. Notably, the addition of payload had no effect on the wind estimation accuracy when using method 1 (Figures 6B-I versus 6D-I), while it amplified the impact of rotor-induced airflow disturbances on sensor measurements (Figures 6B-II versus 6D-II). Similar findings were observed for wind direction estimations (Figure S2).

These analyses demonstrate that the attitude-based method (method 1) can robustly estimate wind variables. The sensor-based method (method 2), with proper calibration, can also achieve accuracy comparable to reference instruments during hovering and low-speed vertical profiling. However, method 2 is not suitable for high-speed vertical profiling due to its high susceptibility to rotor-induced airflow disturbances. These systematic errors were consistently observed across all test configurations. Nevertheless, the successful validation of the attitude-based method substantially enhances the potential for UAV applications in atmospheric research, offering distinct advantages for measurements in locations inaccessible to conventional tower-based systems and in scenarios requiring rapid deployment of mobile platforms.

3.3 Field wind measurements

Field flight experiments were further conducted at a coastal site in Shenzhen, China, to evaluate the wind estimation performance of methods 1 and 2. For vertical profiling, the UAV flight speed was maintained at approximately 0.5 m/s and only ascending flight data were used to minimize the influence of rotor downwash on sensor measurements.

Figure 7 presents the results for UAV hovering data. Strong agreement was observed between the two methods, with median differences of approximately 0.1 m/s for wind speed and less than 10° for wind direction (Figures 7A and S3), confirming the reliability of the UAV attitude-based approach. To further enhance the wind estimation, we implemented a machine learning framework (method 3) using UAV attitude parameters and supplementary flight data as inputs, with corrected wind sensor measurements as the training target. The model achieved excellent predictive performance, with R^2 values exceeding 0.90 for both training and test datasets (Figures 7B and S4). For hovering flights, roll, pitch, yaw, and air pressure were identified as the most important features. When applied to an independent dataset from the meteorological tower flight experiments (Section 3.3), the estimates maintained good agreement with tower measurements (Figure S5).

Similar performance was achieved for UAV vertical flights (Figure S6). In vertical profiling, in addition to the input variables discussed above, vertical flight speed and rotor thrusts became more significant for the machine learning estimates (Figure S6). It should be noted that the rotor thrust information used in this study was only roughly estimated from flight command values issued by the UAV controller, which may introduce significant uncertainty. Future research applying a machine learning approach for wind estimation should therefore seek to incorporate actual rotor thrust or rotor speed data to improve accuracy. Furthermore, as this study focuses only on hovering and vertical flights, horizontal velocity components were not included in the model. For future applications of this approach to horizontal flight, horizontal velocity in the x- and y-directions should also be integrated into the model to account for the UAV motion relative to the air. Nevertheless, the above consistent performance across different validation approaches and flight modes confirms the robustness of the attitude-based methodology and its potential for practical wind measurement applications.

Wind profile estimation offers critical insights into atmospheric pollutant transport and dispersion dynamics. In the same field campaign, we also collected vertical pollutant concentration profiles using a pre-calibrated sensor package (Sniffer V2, Soarability Pte. Ltd.) that was cross-validated against reference instruments at a ground station located 50 m from the flight site. Figure 8 provides an example of representative vertical profiles of wind and pollutants. The diurnal wind profiles were obtained using method 1. The results reveal the crucial influence of wind profiles on pollutant distribution patterns. For instance, persistently low wind speeds were observed throughout the day of August 23, indicating stable atmospheric conditions which were conducive to pollution accumulation. Pollutant concentrations on this day exhibited typical diurnal variations, gradually increasing from morning, peaking in the afternoon due to photochemical activity, and decreasing at night with reduced emissions and photochemical processes. In contrast, September 7 featured strong winds that enhanced pollutant dispersion, resulting in consistently low pollution levels.

The September 14 case demonstrated a complex vertical wind structure, with speeds decreasing from morning to nighttime minima while increasing with height. Pollutant concentrations varied significantly with wind direction changes. Notably, at 19:00, a 180° wind shift transported polluted air masses from the south, sharply increasing observed concentrations. Surface cooling and calm winds on this night created stable stratification, trapping pollutants near the surface and producing distinct vertical gradients. The nocturnal boundary layer height (150-200 m), identifiable from wind and pollutant profiles (Guimarães et al., 2019, 2020; Ye et al., 2021), showed reduced pollutant concentrations at the residual layer due to enhanced wind speed and dispersion. A subsequent wind shift to 360° brought back cleaner northern air, reducing both surface concentrations and vertical gradients. These observations underscore the importance of vertical wind profiling enabled by UAV-attitude-based estimation for understanding atmospheric transport mechanisms and pollution dynamics.

4. Atmospheric Implications

This study develops a wind estimation method based on UAV attitude changes. Validation through wind wall and field experiments demonstrated the reliable performance of the attitude-based approach. Key findings show that payload and wind direction significantly affect attitude responses, highlighting the need for comprehensive training data to improve accuracy. A supervised learning framework was developed to predict wind speed and direction directly from attitude and flight data, achieving accurate and practical field performance. Results from this study also reveal significant rotor-induced interference when using onboard sensors, especially during vertical maneuvers, underscoring the need for pre-deployment sensor calibration. Collectively, these findings demonstrate the strong potential for precise, sensor-free wind field estimation using UAV attitude data.

The attitude-based wind estimation method, while promising, presents several limitations that require future consideration. First, this approach requires establishing accurate relationships between UAV inclination angles and wind speed, which vary across different UAV models. For instance, the platform used in this study showed significant impacts from payload and relative wind direction, a phenomenon not reported by Neumann and Bartholmai (2015) for a different UAV. Consequently, model-specific calibration is essential prior to field deployment. In this work, we selected the DJI M300 RTK (total weight 6.3 kg, maximum payload 2.3 kg) as it represents a class of small-sized rotorcraft capable of carrying scientific payloads such as air pollutant sensors (Li et al., 2025). Different UAV categories present distinct trade-offs. Mini-UAVs (weight < 3 kg), while potentially suitable for low-wind conditions, often lack the payload capacity for full instrumentation and can be overly sensitive to turbulence, increasing estimation uncertainty. Conversely, larger platforms (e.g., agricultural UAVs) are heavier and exhibit a dampened attitude response, making them more stable in high winds; however, in low- to moderate-wind conditions, their significant rotor-induced airflow may dominate the measured signal, degrading fidelity. Thus, platform selection should be guided by the target wind regime and payload requirements, with the understanding that each configuration demands its own calibration.

Additionally, this study identified greater uncertainty in the attitude-based wind speed estimates below 2 m/s under headwind conditions (e.g., 0° to 90°, Figure 3). To enhance accuracy in these low-wind-speed regimes, potential solutions include deploying two UAVs flying in opposite orientations and selecting data from the UAV more sensitive to tailwind conditions, employing a UAV with a flight control system that is more responsive to headwind, or utilizing pre-calibrated onboard sensors. It should be noted that strong vertical winds, for example, from intense thermal convection and terrain-induced uplift, may induce significant platform vibration, and consequently, affect UAV attitude and wind estimation. However, under typical open-field atmospheric conditions where vertical wind speeds are on the order of 0.01 to 0.1 m/s (Lynch and Cassano, 2006; Michaelides et al., 2019), such influences are expected to be minor. The close agreement between the tower-based (or calibrated sensor) measurements and the UAV attitude-based estimates (Figures 6 and 7) further supports this conclusion. Furthermore, the UAV's own rotor-induced vertical velocities, which can exceed several m/s for platforms such as DJI M300 RTK (Li et al., 2025) and are often substantially larger than typical ambient vertical wind speeds, dominate the vertical momentum balance and mask weaker atmospheric updrafts or downdrafts. Nevertheless, future research focused on UAV wind estimation in environments with significant vertical flows, such as urban street canyons, mountainous terrain with intense slope winds, or severe weather fronts, should explicitly account for the influence of vertical winds on UAV dynamics to ensure accurate retrievals.

Finally, creating a comprehensive database linking UAV attitude data to wind measurements across diverse flight conditions (e.g., hovering, horizontal, and vertical flight at varying speeds) and environmental scenarios would be highly valuable. While previous studies have applied machine learning to train wind observation data (e.g., Zhu et al., 2025), they have generally been constrained by single-flight tests or limited datasets, which may not fully capture the variability of UAV responses across different operating environments. In practice, UAV attitude and rotor dynamics are strongly modulated by wind direction, flight mode, and payload configuration, leading to highly nonlinear and platform-specific responses, as demonstrated in this study. In addition, in complex terrains such as urban canyons or under unstable atmospheric conditions, the wind itself can be complex, inducing turbulence and wind shear that significantly affect UAV attitude and may introduce uncertainty in UAV-based wind estimates. A dataset encompassing such varied conditions would enable the training of more advanced AI models, accelerating the development of reliable, attitude-based wind field prediction methods.

In regard to further applications, with the global development of the low-altitude economy (Huang et al., 2024; Saadé et al., 2025; Tan et al., 2025; Zhou, 2025), UAV attitude-based wind estimation has become an essential enabling technology. The sensor-free approach described here uses inherent flight dynamics to generate reliable wind field data, offering advantages in low-altitude operations where conventional methods are limited. Its operational simplicity and cost-effectiveness make it valuable for widespread use in sectors such as urban air mobility, where it can support flight safety by integrating easily into existing UAV systems.

In environmental applications, UAVs provide precise, flexible, and efficient wind measurements with high spatiotemporal resolution. This enables vertical wind profiling, improving the analysis of atmospheric pollutant transport. Such data can help identify pollution sources and inform mitigation strategies, especially in complex urban settings where building layouts and street-level airflow affect air quality. The three-dimensional wind data obtained from UAV measurements can inform urban planning decisions by characterizing how architectural geometries modulate near-surface ventilation efficiency.

Furthermore, the measurement capabilities provide critical data for validating high-resolution weather and climate models, especially for simulating complex urban canopy effects on microscale wind circulation patterns that govern heat dissipation.

Beyond urban research, UAV-based wind estimation opens new opportunities for field studies in natural ecosystems and remote regions. For example, reliable vertical wind profiles can substantially improve the quantification of forest canopy-atmosphere exchange processes, including the dispersion of biogenic volatile organic compounds and greenhouse gases (Jiang et al., 2024; Ye et al., 2021; Ye et al., 2022). Similarly, accurate wind field characterization over coastal and marine environments enhances the interpretation of air-sea exchange, sea-breeze circulation, and the long-range transport of marine aerosols (Zhao et al., 2021).

Through these varied applications, UAV-based wind measurement technology is emerging as an innovative tool that connects the low-altitude economy with environmental science. By delivering spatiotemporally resolved wind data in complex terrains and under diverse atmospheric conditions, the approach not only advances intelligent environmental risk management but also supports sustainable development initiatives and climate adaptation strategies on regional scales.

Supporting Information. The supporting information includes the following items:

- Text S1 Estimation of UAV rotor thrusts
- Table S1 Fitting coefficients for the UAV inclination-wind speed relationships.
- Table S2 Fitting coefficients k and b for wind sensor calibrations under various flight conditions.
- Figure S1 UAV attitude response to a step change in wind speed.
- Figure S2 Comparison between UAV-based wind direction estimates and reference measurements from the meteorological observation tower during vertical flight operations.
- Figure S3 UAV-based wind direction estimation and deviation analysis comparing different methods from the field observation campaign.
- Figure S4 Performance of wind estimation using machine learning algorithms for hovering flights.
- Figure S5 Comparison between UAV-attitude-based wind speed estimates using machine learning algorithms and reference measurements from the meteorological observation tower during hovering flight operations.
- Figure S6 Performance of wind estimation using machine learning algorithms for vertical flights. And comparison between UAV-attitude-based wind speed estimates using machine learning algorithms and reference measurements from the meteorological observation tower during vertical flight operations.

Corresponding Author. Jianhuai Ye (yejh@sustech.edu.cn), ORCID: 0000-0002-9063-3260

Author Contribution. J.Y. designed the research; D.C., W.S., S.J., Y.L. and J.Y. conducted wind wall and meteorological tower flight experiments; S.J. and J.Y. performed the UAV field campaign; D.C. and J.Y. analyzed the data and wrote the original manuscript; all authors contributed to the data interpretation and manuscript writing.

Competing Interest. The authors declare no competing financial interest.

Acknowledgments. This work was funded by National Key Research and Development Program of China (2024YFC3714300), National Natural Science Foundation of China (Nos. 42375091, U24A20515, and 42105098), and Shenzhen Science and Technology Program (JCYJ20241202152804007, KQTD20240729102048052, and SGDX20230116091648011). High Level of Special Funds (G03050K001) from Southern University of Science and Technology is acknowledged.

References

Achermann, F., Stastny, T., Danciu, B., Kolobov, A., Chung, J. J., Siegwart, R., and Lawrance, N.: WindSeer: real-time volumetric wind prediction over complex terrain aboard a small uncrewed aerial vehicle, Nat. Commun., 15, 3507, https://doi.org/10.1038/s41467-024-47778-4, 2024.

Ahmed, Z., Halefom, M. H., and Woolsey, C.: Tutorial review of indirect wind estimation methods using small uncrewed air vehicles, J. Aerosp. Inf. Syst., 21, 667-683, https://doi.org/10.2514/1.I011345, 2024.

Alfonso-Corcuera, D., Ogueta-Gutiérrez, M., Fernández-Soler, A., González-Bárcena, D., and Pindado, S.: Measuring relative wind speeds in stratospheric balloons with cup anemometers: the TASEC-lab mission, Sensors, 22, 5575, https://doi.org/10.3390/s22155575, 2022.

Alizadeh, O., Abniki, M., Babaei, M., and Irannejad, P.: Climatology and the dynamic mechanism of the levar wind and dust events in eastern Iran, Int. J. Climatol., 42, 9288-9303, https://doi.org/10.1002/joc.7818, 2022.

Asher, E., Hills, A. J., Hornbrook, R. S., Shertz, S., Gabbard, S., Stephens, B. B., Helmig, D., and Apel, E. C.: Unpiloted aircraft system instrument for the rapid collection of whole air samples and measurements for environmental monitoring and air quality studies, Environ. Sci. Technol., 55, 5657-5667, https://doi.org/10.1021/acs.est.0c07213, 2021.

Batista, C. E., Ye, J., Ribeiro, I. O., Guimarães, P. C., Medeiros, A. S. S., Barbosa, R. G., Oliveira, R. L., Duvoisin, S., Jardine, K. J., Gu, D., Guenther, A. B., McKinney, K. A., Martins, L. D., Souza, R. A. F., and Martin, S. T.: Intermediate-scale horizontal isoprene concentrations in the near-canopy forest atmosphere and implications for emission heterogeneity, Proc. Natl. Acad. Sci., 116, 19318-19323, https://doi.org/10.1073/pnas.1904154116, 2019.

Brosy, C., Krampf, K., Zeeman, M., Wolf, B., Junkermann, W., Schäfer, K., Emeis, S., and Kunstmann, H.: Simultaneous multicopter-based air sampling and sensing of meteorological variables, Atmos. Meas. Tech., 10, 2773-2784, https://doi.org/10.5194/amt-10-2773-2017, 2017.

Curbelo, J. and Rypina, I. I.: A three dimensional Lagrangian analysis of the smoke plume from the 2019/2020 Australian wildfire event, J. Geophys. Res. Atmos., 128, e2023JD039773, https://doi.org/10.1029/2023JD039773, 2023.

Diasinos, S., Beves, C., and Barber, T.: Alignment technique for three-dimensional laser doppler anemometry, Meas. Sci. Technol., 24, 17001, https://doi.org/10.1088/0957-0233/24/1/017001, 2013.

Ding, L. and Wang, Z.: A robust control for an aerial robot quadrotor under wind gusts, J. Robot., 2018, 1-8, https://doi.org/10.1155/2018/5607362, 2018.

Feng, Y., Fu, D., Zhao, Z., Zong, W., Yu, T., Sheng, Z., and Zhu, Y.: An overview of spaceborne atmospheric wind field measurement with passive optical remote sensing, Acta Opt. Sin., 43, 0601011, https://doi.org/10.3788/AOS221462, 2023.

Gaeta Lopes, G. M., da Silva Junior, D. P., de Franca, J. A., de Morais Franca, M. B., Ribeiro, L. de S., Moreira, M., and Elias, P.: Development of 3-D ultrasonic anemometer with nonorthogonal geometry for the determination of high-intensity winds, IEEE Trans. Instrum. Meas., 66, 2836-2844, https://doi.org/10.1109/TIM.2017.2714438, 2017.

González-Rocha, J., Woolsey, C. A., Sultan, C., and De Wekker, S. F. J.: Sensing wind from quadrotor motion, J. Guid. Control Dyn., 42, 836-852, https://doi.org/10.2514/1.G003542, 2019.

González-Rocha, J., Bilyeu, L., Ross, S. D., Foroutan, H., Jacquemin, S. J., Ault, A. P., and Schmale, D. G.: Sensing atmospheric flows in aquatic environments using a multirotor small uncrewed aircraft system (sUAS), Environ. Sci. Atmos., 3, 305-315, https://doi.org/10.1039/D2EA00042C, 2023.

Guimarães, P., Ye, J., Batista, C., Barbosa, R., Ribeiro, I., Medeiros, A., Souza, R., and Martin, S. T.: Vertical profiles of ozone concentration collected by an unmanned aerial vehicle and the mixing of the nighttime boundary layer over an Amazonian urban area, Atmosphere, 10, 599, https://doi.org/10.3390/atmos10100599, 2019.

Guimarães, P., Ye, J., Batista, C., Barbosa, R., Ribeiro, I., Medeiros, A., Zhao, T., Hwang, W.-C., Hung, H.-M., Souza, R., and T. Martin, S.: Vertical profiles of atmospheric species concentrations and nighttime boundary layer structure in the dry season over an urban environment in central Amazon collected by an unmanned aerial vehicle, Atmosphere, 11, 1371, https://doi.org/10.3390/atmos11121371, 2020.

Guo, J., Miao, Y., Zhang, Y., Liu, H., Li, Z., Zhang, W., He, J., Lou, M., Yan, Y., Bian, L., and Zhai, P.: The climatology of planetary boundary layer height in China derived from radiosonde and reanalysis data, Atmos. Chem. Phys., 16, 13309-13319, https://doi.org/10.5194/acp-16-13309-2016, 2016.

Han, D., Kim, S., and Park, S.: Two-dimensional ultrasonic anemometer using the directivity angle of an ultrasonic sensor, Microelectron. J., 39, 1195-1199, https://doi.org/10.1016/j.mejo.2008.01.090, 2008.

Hauser, D., Abdalla, S., Ardhuin, F., Bidlot, J.-R., Bourassa, M., Cotton, D., Gommenginger, C., Evers-King, H., Johnsen, H., Knaff, J., Lavender, S., Mouche, A., Reul, N., Sampson, C., Steele, E. C. C., and Stoffelen, A.: Satellite remote sensing of surface winds, waves, and currents: where are we now?, Surv. Geophys., 44, 1357-1446, https://doi.org/10.1007/s10712-023-09771-2, 2023.

Horton, D. E., Skinner, C. B., Singh, D., and Diffenbaugh, N. S.: Occurrence and persistence of future atmospheric stagnation events, Nat. Clim. Change, 4, 698-703, https://doi.org/10.1038/nclimate2272, 2014.

Huang, H., Su, J., and Wang, F.-Y.: The potential of low-altitude airspace: the future of urban air transportation, IEEE Trans. Intell. Veh., 9, 5250-5254, https://doi.org/10.1109/TIV.2024.3483889, 2024.

Jiang, S., Wang, Y., Huang, X., Liu, B., Nie, D., Ge, Y., Ma, L., Wang, Q., Wang, J., Ma, Y., Jiang, S., Shu, Z., Zhang, Y., Sun, J., Wu, C., Ge, X., Zhu, L., Shen, H., Wang, C., Zheng, Y., Fu, T.-M., Yang, X., Li, Y. J., Chen, Q., and Ye, J.: Characteristics of nocturnal boundary layer over a subtropical forest: implications for the dispersion and fate of atmospheric species, Environ. Sci. Technol., 58, 23075-23087, https://doi.org/10.1021/acs.est.4c05051, 2024.

Jung, S.: Precision landing of unmanned aerial vehicle under wind disturbance using derivative sliding mode nonlinear disturbance observer-based control method, Aerospace, 11, 265, https://doi.org/10.3390/aerospace11040265, 2024.

Knöller, W., Bagheri, G., Von Olshausen, P., and Wilczek, M.: Analysis of the measurement uncertainty for a 3D wind lidar, Atmos. Meas. Tech., 17, 6913-6931, https://doi.org/10.5194/amt-17-6913-2024, 2024.

Lee, B.: Review of the present status of optical fiber sensors, Opt. Fiber Technol., 9, 57-79, https://doi.org/10.1016/S1068-5200(02)00527-8, 2003.

Lei, Y. and Lin, R.: Effect of wind disturbance on the aerodynamic performance of coaxial rotors during hovering, Meas. Control, 52, 665-674, https://doi.org/10.1177/0020294019834961, 2019.

Li, Y., Zhang, C., Su, W., Jiang, S., Nie, D., Wang, Y., Wang, Y., He, H., Chen, Q., Martin, S. T., and Ye, J.: Copter-type UAV-based sensing in atmospheric chemistry: recent advances, applications, and future perspectives, Environ. Sci. Technol., 59, 13532-13550, https://doi.org/10.1021/acs.est.5c00074, 2025.

Liu, J., Zhao, Z., Fang, Z., Li, Y., and Du, L.: Correction of error of airborne anemometers caused by self-excited air turbulence, Sensors, 23, 4288, https://doi.org/10.3390/s23094288, 2023.

Lynch, A. H. and Cassano, J. J.: Applied Atmospheric Dynamics, John Wiley & Sons, Hoboken, NJ, USA, 2006.

Michaelides, S., Lane, J., and Kasparis, T.: Effect of vertical air motion on disdrometer derived Z-R coefficients, Atmosphere, 10, 77-98, https://doi.org/10.3390/atmos10020077, 2019.

Neumann, P. P. and Bartholmai, M.: Real-time wind estimation on a micro unmanned aerial vehicle using its inertial measurement unit, Sens. Actuators Phys., 235, 300-310, https://doi.org/10.1016/j.sna.2015.09.036, 2015.

Otsuka, H., Sasaki, D., and Nagatani, K.: Reduction of the head-up pitching moment of small quad-rotor unmanned aerial vehicles in uniform flow, Int. J. Micro Air Veh., 10, 85-105, https://doi.org/10.1177/1756829317745318, 2018.

Palomaki, R. T., Rose, N. T., Van Den Bossche, M., Sherman, T. J., and De Wekker, S. F. J.: Wind estimation in the lower atmosphere using multirotor aircraft, J. Atmos. Ocean. Technol., 34, 1183-1191, https://doi.org/10.1175/JTECH-D-16-0177.1, 2017.

Pindado, S., Cubas, J., and Sorribes-Palmer, F.: The cup anemometer, a fundamental meteorological instrument for the wind energy industry. Research at the IDR/UPM institute, Sensors, 14, 21418-21452, https://doi.org/10.3390/s141121418, 2014.

Richiardone, R., Manfrin, M., Ferrarese, S., Francone, C., Fernicola, V., Gavioso, R. M., and Mortarini, L.: Influence of the sonic anemometer temperature calibration on turbulent heat-flux measurements, Bound.-Layer Meteorol., 142, 425-442, https://doi.org/10.1007/s10546-011-9688-z, 2012.

Saadé, R. G., Hao, L., and Kuusiholma, T.: Global governance & aerospace - the need for a management-integrated air and space education paradigm, J. Space Saf. Eng., 12, 17-27, https://doi.org/10.1016/j.jsse.2025.04.003, 2025.

Salmabadi, H., Khalidy, R., and Saeedi, M.: Transport routes and potential source regions of the Middle Eastern dust over Ahvaz during 2005-2017, Atmos. Res., 241, 104947, https://doi.org/10.1016/j.atmosres.2020.104947, 2020.

Shan, Z., Xie, X., and Liu, X.: Wind speed and direction measurement based on three mutually transmitting ultrasonic sensors, IEEE Geosci. Remote Sens. Lett., 20, 8000205, https://doi.org/10.1109/LGRS.2023.3236005, 2023.

Sikkel, L. N. C., de Croon, G. C. H. E., De Wagter, C., and Chu, Q. P.: A novel online model-based wind estimation approach for quadrotor micro air vehicles using low cost MEMS IMUs, in: 2016 IEEE/RSJ International Conference on Intelligent Robots and Systems (IROS), pp. 2141-2146, https://doi.org/10.1109/IROS.2016.7759336, 2016.

Tan, H., Guo, Z., Yan, J., Zhang, D., Chen, Y., and Zhang, H.: Advancing low-carbon smart cities: leveraging UAVs-enabled low-altitude economy principles and innovations, Renew. Sustain. Energy Rev., 222, 115942, https://doi.org/10.1016/j.rser.2025.115942, 2025.

Tominaga, Y. and Shirzadi, M.: Wind tunnel measurement of three-dimensional turbulent flow structures around a building group: impact of high-rise buildings on pedestrian wind environment, Build. Environ., 206, 108389, https://doi.org/10.1016/j.buildenv.2021.108389, 2021.

Wang, H.-J. and Chen, H.-P.: Understanding the recent trend of haze pollution in eastern China: roles of climate change, Atmos. Chem. Phys., 16, 4205-4211, https://doi.org/10.5194/acp-16-4205-2016, 2016.

Yang, J., Wu, L., Li, R., Liu, X., and Tao, C.: Effects of surrounding urban morphology and wind direction on hazardous gas dispersion from chemical plants: morphological analysis and fluid dynamics insights into industry-urban interactions, Phys. Fluids, 37, 27103, https://doi.org/10.1063/5.0251016, 2025a.

Yang, Y., Russell, L. M., Lou, S., Liu, Y., Singh, B., and Ghan, S. J.: Rain-aerosol relationships influenced by wind speed, Geophys. Res. Lett., 43, 2267-2274, https://doi.org/10.1002/2016GL067770, 2016.

Yang, Y., Russell, L. M., Lou, S., Liao, H., Guo, J., Liu, Y., Singh, B., and Ghan, S. J.: Dust-wind interactions can intensify aerosol pollution over eastern China, Nat. Commun., 8, 15333, https://doi.org/10.1038/ncomms15333, 2017.

Yang, Y., Zhang, Y., Han, T., Xie, C., Liu, Y., Huang, Y., Zhou, J., Sun, H., Zhao, D., Zhang, K., and Li, S.-M.: A correction algorithm for rotor-induced airflow and flight attitude changes during three-dimensional wind speed measurements made from a rotary unoccupied aerial vehicle, Atmos. Meas. Tech., 18, 3035-3050, https://doi.org/10.5194/amt-18-3035-2025, 2025b.

Ye, J., Batista, C. E., Guimarães, P. C., Ribeiro, I. O., Vidoudez, C., Barbosa, R. G., Oliveira, R. L., Ma, Y., Jardine, K. J., Surratt, J. D., Guenther, A. B., Souza, R. A. F., and Martin, S. T.: Near-canopy horizontal concentration heterogeneity of semivolatile oxygenated organic compounds and implications for 2-methyltetrols primary emissions, Environ. Sci. Atmos., 1, 8-20, https://doi.org/10.1039/D0EA00006J, 2021.

Ye, J., Batista, C. E., Zhao, T., Campos, J., Ma, Y., Guimarães, P., Ribeiro, I. O., Medeiros, A. S. S., Stewart, M. P., Vilà-Guerau De Arellano, J., Guenther, A. B., Souza, R. A. F. D., and Martin, S. T.: River winds and transport of forest volatiles in the Amazonian riparian ecoregion, Environ. Sci. Technol., 56, 12667-12677, https://doi.org/10.1021/acs.est.1c08460, 2022.

Zhao, T., Ye, J., Ribeiro, I. O., Ma, Y., Hung, H.-M., Batista, C. E., Stewart, M. P., Guimarães, P. C., Vilà-Guerau De Arellano, J., De Souza, R. A. F., Guenther, A. B., and Martin, S. T.: River winds and pollutant recirculation near the Manaus city in the central Amazon, Commun. Earth Environ., 2, 205, https://doi.org/10.1038/s43247-021-00277-6, 2021.

Zhou, Y.: Unmanned aerial vehicles based low-altitude economy with lifecycle techno-economic-environmental analysis for sustainable and smart cities, J. Clean. Prod., 499, 145050, https://doi.org/10.1016/j.jclepro.2025.145050, 2025.

Zhu, S., Zhao, T., Zhang, H., Chen, Y., Yang, D., Liu, Y., and Cao, J.: UAVs' flight dynamics is all you need for wind speed and direction measurement in air, Drones, 9, 466, https://doi.org/10.3390/drones9070466, 2025.

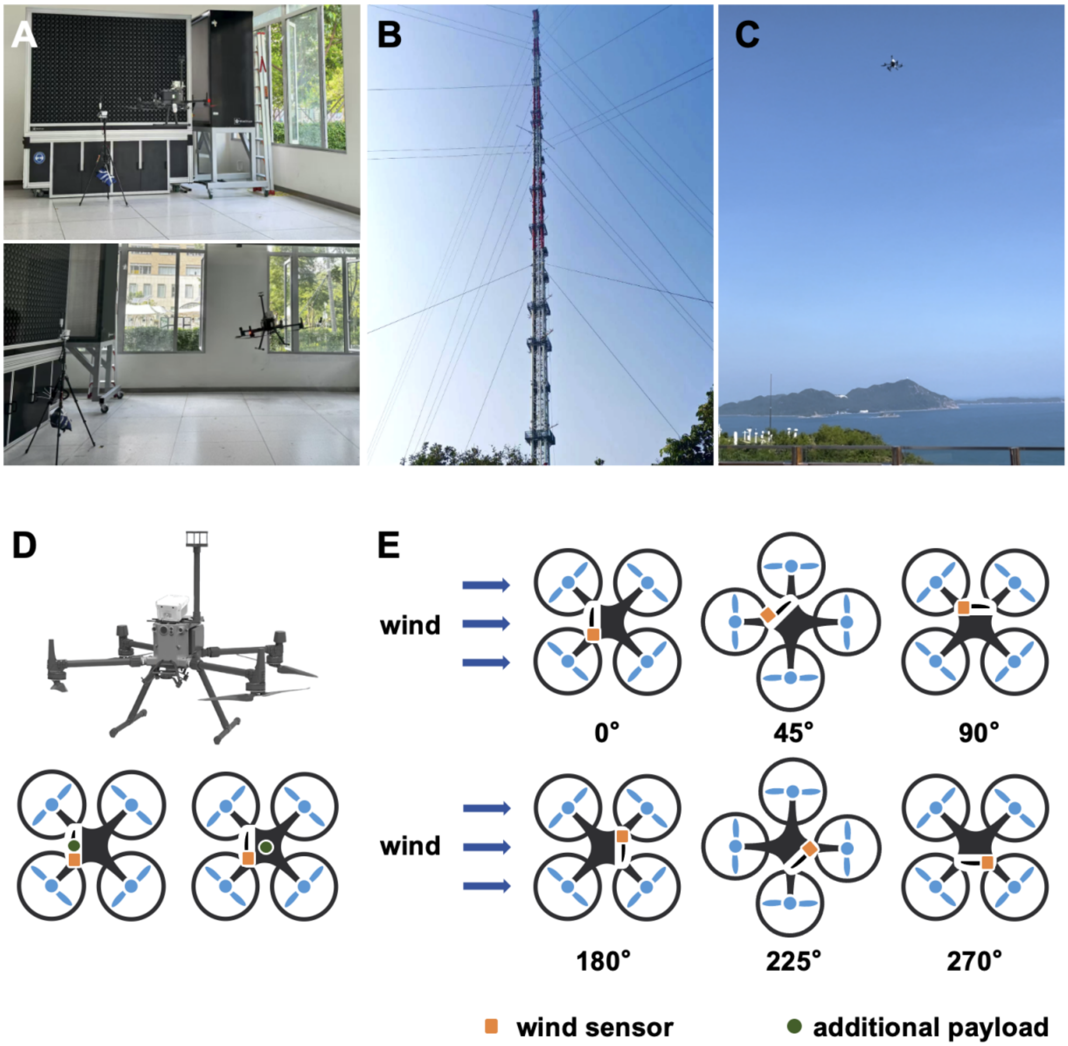

Figure 1 UAV flights conducted in a wind wall laboratory (A), at a meteorological observation tower (B), and at a coastal site (C). Picture and schematic diagrams of UAV payload configuration (D) and UAV flights under different relative wind directions (E).

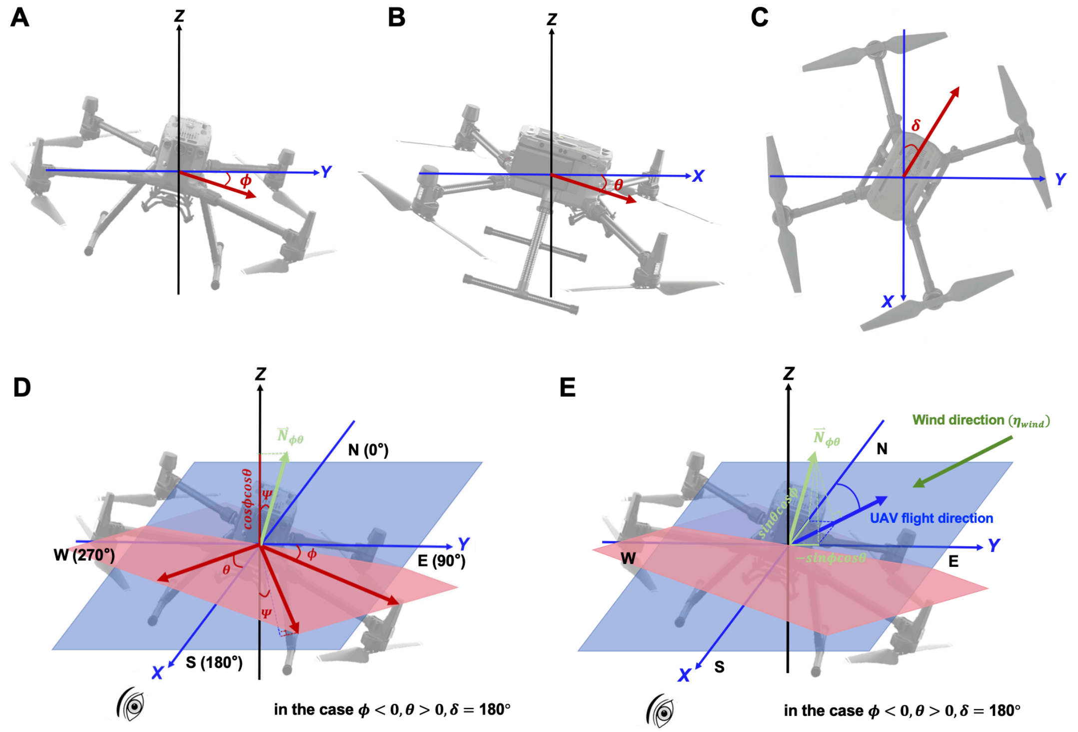

Figure 2 Schematic diagrams of UAV attitude coordinates. Panels depict (A) roll (ϕ), (B) pitch (θ), (C) yaw (δ), (D) UAV inclination angle (Ψ), and (E) the relationship between UAV flight direction and wind direction (η_{wind}). In panels (D) and (E), the example case corresponds to $\phi < 0$, $\theta > 0$, and $\delta = 180°$. The blue plane represents the ground horizontal plane, while the red plane represents the UAV's inclined plane. $\vec{N}_{\phi\theta}$ denotes the normal vector perpendicular to the UAV's inclined plane.

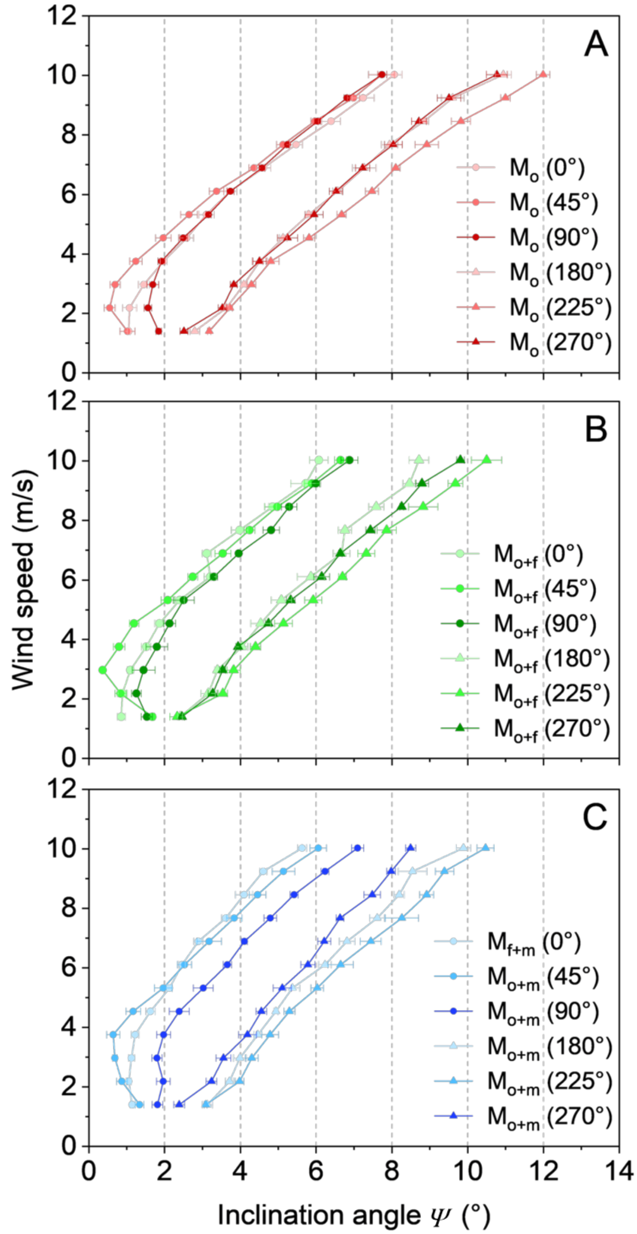

Figure 3 Relationship between UAV inclination angle and wind speed under varying payload (A: default, B: additional front-top payload, C: additional central-top payload) and wind direction (0°, 45°, 90°, 180°, 225°, and 270°) conditions. The payload configurations and relative wind directions are illustrated in Figure 2. The relationships are characterized by power function fits, with coefficients for each flight scenario provided in Table S1.

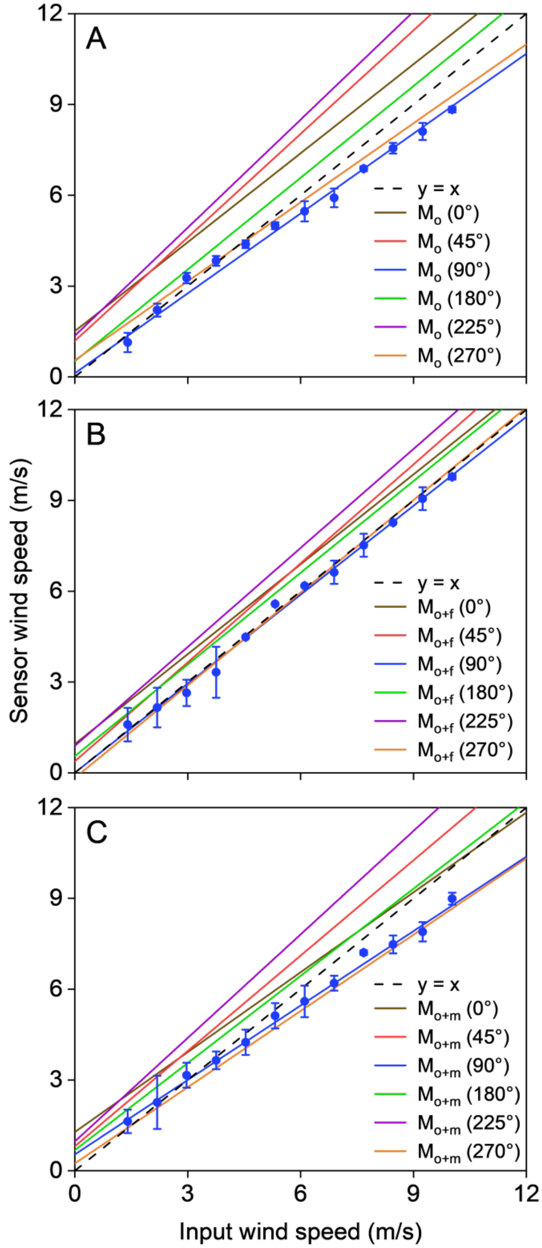

Figure 4 Relationship between input wind speed and sensor-measured wind speed under varying payload (A: default, B: additional front-top payload, C: additional central-top payload) and wind direction (0°, 45°, 90°, 180°, 225°, and 270°) conditions. Both measurements and fitted curves are shown for 90° relative wind direction scenarios, while only fitted curves are presented for other directions. Corresponding fitting parameters are provided in Table S2.

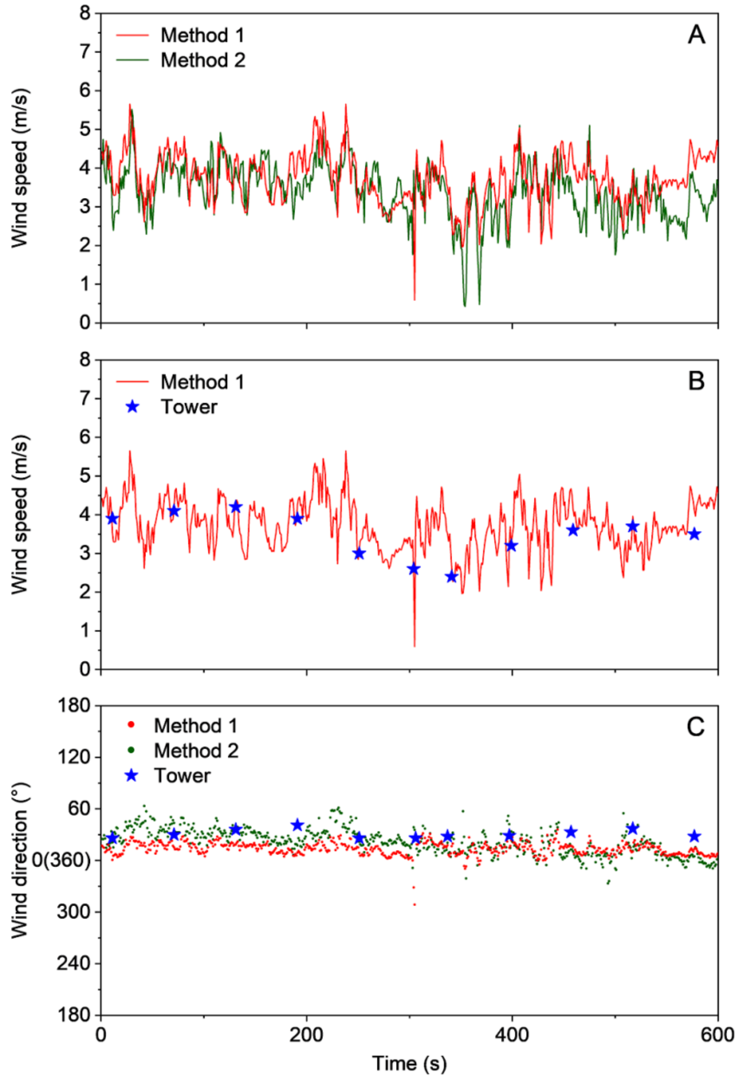

Figure 5 Comparison between UAV-based wind speed estimates (from methods 1 and 2) and reference measurements from the meteorological observation tower during hovering flight operations.

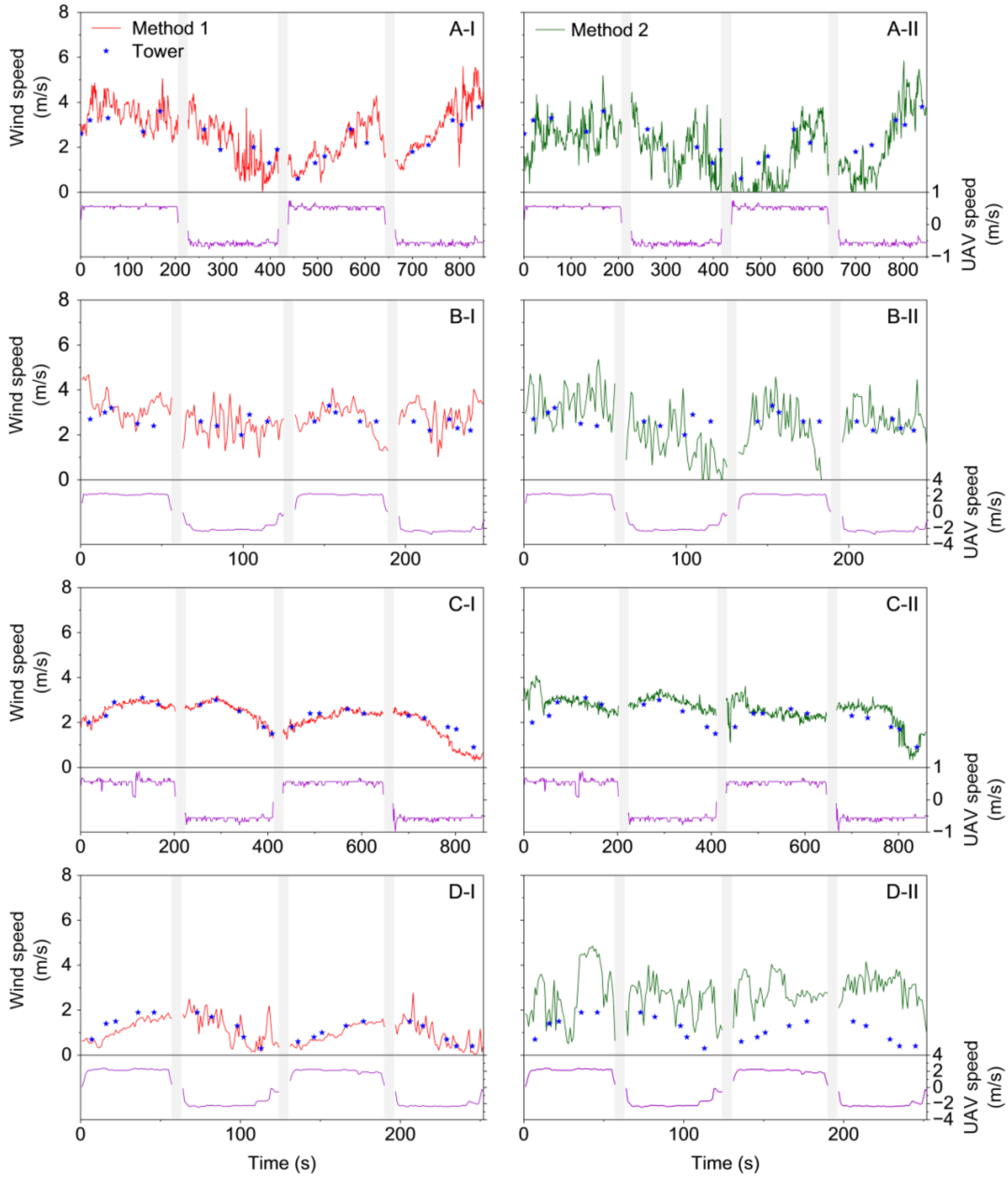

Figure 6 Comparison between UAV-based wind speed estimates and reference measurements from the meteorological observation tower during vertical flight operations: ascending and descending at 0.5 m/s (A) and 2 m/s (B) with default payload, and at 0.5 m/s (C) and 2 m/s (D) with additional front-top payload. Gray shaded areas indicate hovering periods.

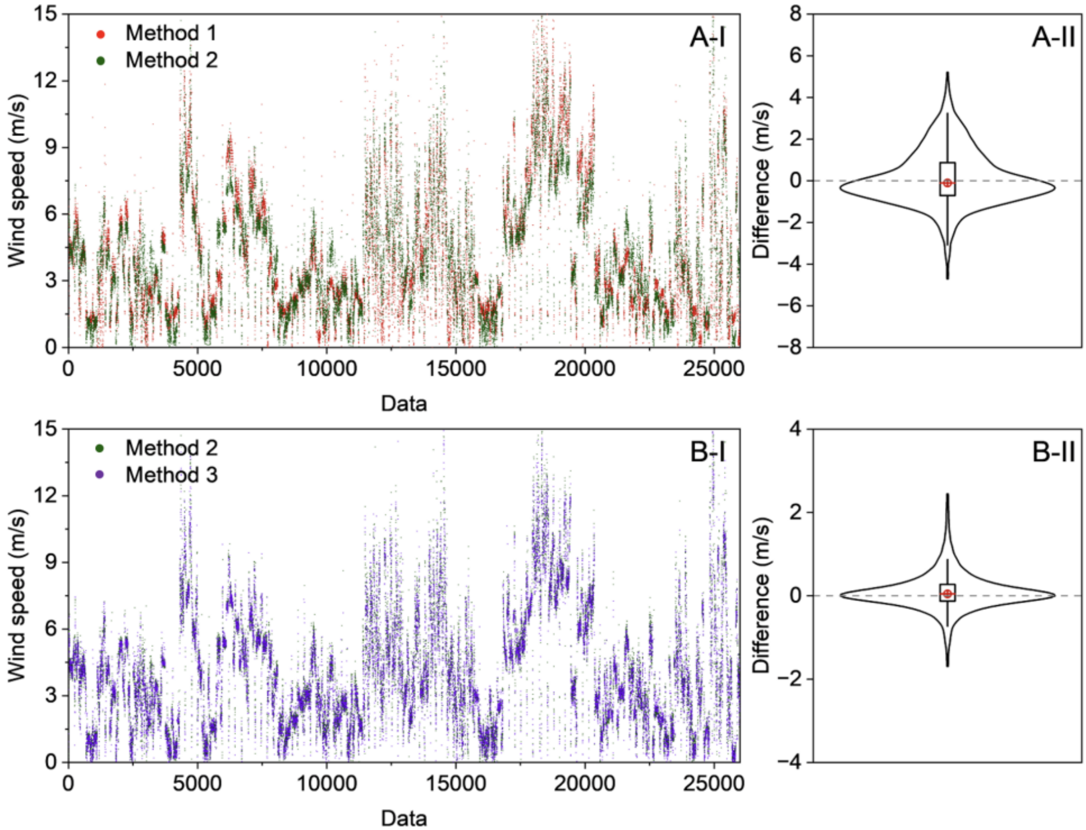

Figure 7 UAV-based wind speed estimation and deviation analysis comparing methods 1 versus 2 (A-I, A-II) and methods 2 versus 3 (B-I, B-II) from the field observation campaign.

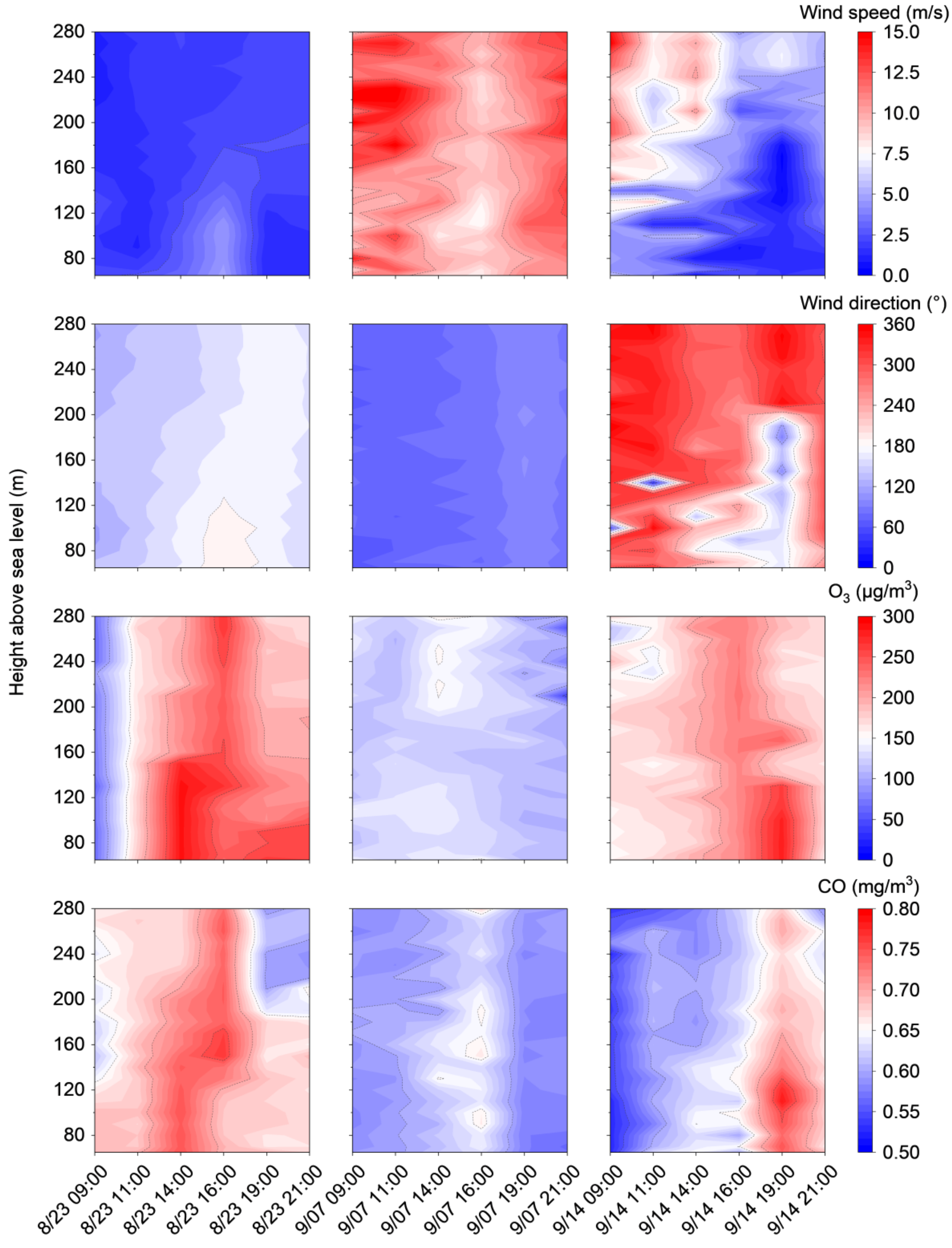

Figure 8 2-D contour plots of the vertical profiles of wind speed, wind direction, O_3 and CO concentrations measured on August 23, September 7, and September 14 of 2022, respectively. All data represent 10-s averages.